P-Glycoprotein (ABCB1) Inhibits the Influx and Increases the Efflux of ^{11}C-Metoclopramide Across the Blood–Brain Barrier: A PET Study on Nonhuman Primates

Sylvain Auvity[1], Fabien Caillé[1], Solène Marie[1], Catriona Wimberley[1], Martin Bauer[2], Oliver Langer[2–4], Irène Buvat[1], Sébastien Goutal[1,5], and Nicolas Tournier[1]

[1]UMR 1023 IMIV, Service Hospitalier Frédéric Joliot, CEA, INSERM, Université Paris Sud, CNRS, Université Paris-Saclay, Orsay, France; [2]Department of Clinical Pharmacology, Medical University of Vienna, Vienna, Austria; [3]Division of Nuclear Medicine, Department of Biomedical Imaging and Image-Guided Therapy, Medical University of Vienna, Vienna, Austria; [4]Biomedical Systems, Center for Health and Bioresources, AIT Austrian Institute of Technology GmbH, Seibersdorf, Austria; and [5]MIRCen, CEA and CNRS-UMR9199, Université Paris Sud, Fontenay-aux-Roses, France

PET imaging using radiolabeled avid substrates of the ATP-binding cassette (ABC) transporter P-glycoprotein (ABCB1) has convincingly revealed the role of this major efflux transporter in limiting the influx of its substrates from blood into the brain across the blood–brain barrier (BBB). Many drugs, such as metoclopramide, are weak ABCB1 substrates and distribute into the brain even when ABCB1 is fully functional. In this study, we used kinetic modeling and validated simplified methods to highlight and quantify the impact of ABCB1 on the BBB influx and efflux of ^{11}C-metoclopramide, as a model of a weak ABCB1 substrate, in nonhuman primates. **Methods:** The regional brain kinetics of a tracer dose of ^{11}C-metoclopramide (298 ± 44 MBq) were assessed in baboons using PET without ($n = 4$) or with ($n = 4$) intravenous coinfusion of the ABCB1 inhibitor tariquidar (4 mg/kg/h). Metabolite-corrected arterial input functions were generated to estimate the regional volume of distribution (V_T), as well as the influx (K_1) and efflux (k_2) rate constants, using a 1-tissue-compartment model. Modeling outcome parameters were correlated with image-derived parameters, that is, areas under the regional time–activity curves (AUCs) from 0 to 30 min and from 30 to 60 min (SUV·min) and the elimination slope (k_E; min^{-1}) from 30 to 60 min. **Results:** Tariquidar significantly increased the brain distribution of ^{11}C-metoclopramide (V_T = 4.3 ± 0.5 mL/cm^3 and 8.7 ± 0.5 mL/cm^3 for baseline and ABCB1 inhibition conditions, respectively, $P < 0.001$), with a 1.28-fold increase in K_1 ($P < 0.05$) and a 1.64-fold decrease in k_2 ($P < 0.001$). The effect of tariquidar was homogeneous across different brain regions. The parameters most sensitive to ABCB1 inhibition were V_T (2.02-fold increase) and AUC from 30 to 60 min (2.02-fold increase). V_T correlated significantly ($P < 0.0001$) with AUC from 30 to 60 min ($r^2 = 0.95$), with AUC from 0 to 30 min ($r^2 = 0.87$), and with k_E ($r^2 = 0.62$). **Conclusion:** ^{11}C-metoclopramide PET imaging revealed the relative importance of both the influx hindrance and the efflux enhancement components of ABCB1 in a relevant model of the human BBB. The overall impact of ABCB1 on drug delivery to the brain can be noninvasively estimated from image-derived outcome parameters without the need for an arterial input function.

Key Words: ^{11}C-metoclopramide; P-glycoprotein; ABC transporters; blood-brain barrier; positron emission tomography; influx hindrance; efflux enhancement

J Nucl Med 2018; 59:1609–1615
DOI: 10.2967/jnumed.118.210104

P-glycoprotein (ABCB1) is the most studied ATP-binding cassette (ABC) transporter expressed at the luminal (blood-facing) side of endothelial cells forming the blood–brain barrier (BBB) (*1,2*). At the cellular level, ABCB1 mediates the efflux of a large variety of compounds from the intracellular space. At the BBB, ABCB1 was shown to limit exposure of the brain to many xenobiotics and to protect the brain against potentially neurotoxic substances by restricting their influx from the blood into the brain parenchyma (*3*). The downside of this protective function is that ABCB1 is a bottleneck in drug development because it reduces the number of effective drug candidates to treat central nervous system (CNS) diseases (*4*). ABCB1-mediated transport is now systematically considered to be a parameter explaining low brain distribution of new chemical entities (*5*).

However, many marketed CNS-active drugs were shown to be weak ABCB1 substrates, including some antiepileptic drugs (*6*), opioids (*7*), antidepressants (*8*), and neuroleptics (*9*). These compounds are considered weak ABCB1 substrates because their permeability is sufficient to cross the BBB and distribute into the brain parenchyma, even when ABCB1 is fully functional (*10–12*). It can be hypothesized that for such drugs, the impact of ABCB1 on brain distribution may differ from that of avid ABCB1 substrates, with ABCB1 effectively inhibiting uptake of drugs from the blood into the brain, resulting in very low baseline brain distribution (influx hindrance) (*13*). Once inside the brain, weak ABCB1 substrates may undergo ABCB1-mediated efflux transport across the BBB. ABCB1 may thus control the clearance of its substrates from the brain into the blood (efflux enhancement). Under such conditions, ABCB1 would act as a detoxifying system, thus adding a new role for ABCB1 in controlling drug exposure to the brain after initial uptake (*13*).

A powerful method to study ABCB1 function in vivo at the human BBB is PET imaging in combination with radiolabeled

Received Feb. 20, 2018; revision accepted Apr. 23, 2018.
For correspondence or reprints contact: Nicolas Tournier, CEA, DRF, Joliot, Service Hospitalier Frédéric Joliot, Orsay, F-91401, France.
E-mail: nicolas.tournier@cea.fr
Published online May 10, 2018.

ABCB1 substrate radiotracers (*2*). The most commonly used ABCB1 probes for PET are racemic ^{11}C-verapamil, (*R*)-^{11}C-verapamil, and ^{11}C-*N-desmethyl*-loperamide. These radiotracers are avid ABCB1 substrates, with a high transport rate, and show very low brain uptake when ABCB1 is functional. In humans, their brain uptake increased when ABCB1 was pharmacologically inhibited, thus providing convincing clinical data on the impact of this functional component of the BBB in vivo (*2,14,15*). These radiotracers may, however, not be representative of most clinically used CNS-active drugs. Better insight into the role of ABCB1 in controlling the brain distribution of CNS-active drugs is much needed to improve our understanding of the impact of ABCB1 on the variability in response to CNS-active drugs, in terms of both efficacy and adverse effects (*16*).

Metoclopramide is commonly prescribed as an antiemetic drug. Frequent CNS effects have been reported, suggesting substantial brain distribution (*17,18*). Metoclopramide is a moderate substrate of both human and rodent ABCB1 (12). We have shown the feasibility of PET imaging with ^{11}C-metoclopramide to measure in vivo ABCB1 function at the rat BBB (*19*).

In the present study, ^{11}C-metoclopramide PET imaging was performed on nonhuman primates, an animal model that more closely resembles humans in terms of ABCB1 expression levels at the BBB than rodents (*20*). Compartmental pharmacokinetic modeling was performed to highlight and quantify the specific contribution of ABCB1 to the BBB crossing and subsequent exposure to brain regions of this model CNS-active, moderate ABCB1 substrate. Simplified methods for quantification of ABCB1 function at the BBB, which do not require arterial blood sampling, were developed and validated.

MATERIALS AND METHODS

Animals

All animal-use procedures were in accordance with the recommendations of the European Community (86/809/CEE) and the French National Committees (law 87/848) for the care and use of laboratory animals. The experimental protocol was validated by a local ethics committee for animal use (CETA/APAFIS 892). Animal experiments were performed on 4 adult male *Papio anubis* baboons (27.58 ± 1.33 kg in weight during the study) obtained from Celphedia, Station of Primatology.

Chemicals and Radiochemicals

Tariquidar used for ABCB1 inhibition was purchased from ERAS Labo. Tariquidar solutions for intravenous injection (3 mg/mL) were freshly prepared on the day of the experiment by dissolving tariquidar dimesylate 2.35 H_2O (~300 mg) in a 5% (w/v) glucose solution (50 mL) followed by dilution with sterile water (50 mL). Ready-to-inject ^{11}C-metoclopramide (4-amino-5-chloro-*N*-(2-(diethylamino)ethyl)-2-^{11}C-methoxybenzamide) more than 99% radiochemically pure was prepared and controlled as previously described (*19,21*).

Experimental Conditions

Four baboons underwent 2 ^{11}C-metoclopramide PET scans. ^{11}C-metoclopramide brain kinetics were compared in the absence (baseline scan) and presence of pharmacologic ABCB1 inhibition, achieved with a concurrent intravenous infusion of tariquidar (inhibition scan). The tariquidar infusion protocol was adapted from a clinically validated protocol (*14*). Tariquidar was infused at a dose of 4 mg/kg/h (37.5 mL/h). The infusion started 1 h before radiotracer injection and was continued during the entire PET acquisition. One baboon underwent a third PET experiment with ^{11}C-metoclopramide coinjected with the maximal clinical dose of unlabeled metoclopramide (0.5 mg/kg of a 10 mg/2 mL solution; Laboratoire Renaudin) (Supplemental Fig. 1; supplemental materials are available at http://jnm.snmjournals.org).

Imaging Experiments

First, each baboon underwent a T1-weighted brain MR scan using an Achieva 1.5-T scanner (Philips Healthcare) under ketamine anesthesia (10 mg/kg, intramuscularly; Virbac).

PET experiments were performed on an HR+ Tomograph (Siemens Healthcare), with the animal anesthetized and monitored as previously described (*22*). The animal received ketamine (10 mg/kg, intramuscularly) to induce anesthesia. Once the animal was intubated, venous catheters were inserted for radiotracer injection (sural vein), propofol infusion (sural vein), and tariquidar infusion (brachial vein). Another catheter was inserted into the femoral artery for arterial blood sampling. The animal was positioned under the camera before administration of an intravenous bolus of propofol (2 mL) followed by a 16–22 mL/h intravenous infusion under oxygen ventilation.

The animal was intravenously injected with ^{11}C-metoclopramide (298 ± 44 MBq; 5.6 ± 3.1 μg). A dynamic PET acquisition (60 min) was performed over the brain with the animal supine.

Arterial Input Function and Metabolism

During the PET acquisition, arterial blood samples (0.5 mL) were withdrawn at selected times after radiotracer injection. Samples were centrifuged (5 min, 2,054*g*, 4°C) and the supernatant (200 μL) was counted for total radioactivity.

Additional plasma samples were withdrawn to measure the percentage of parent (unmetabolized) using high-performance liquid chromatography (HPLC). Time–activity curves of parent ^{11}C-metoclopramide in plasma were expressed as SUV ([radioactivity/mL of plasma/injected radioactivity] × body weight). Plasma exposure to parent ^{11}C-metoclopramide was estimated under all tested conditions by calculating the area under the time–activity curve (AUC) in plasma.

Dedicated arterial plasma samples were withdrawn immediately before ^{11}C-metoclopramide injection to assess ^{11}C-metoclopramide binding to plasma proteins. The fraction of ^{11}C-metoclopramide that was not bound to baboon plasma proteins (f_P) was measured as previously described (*23*).

Imaging Data Analysis

PET images were reconstructed as previously described (*24*). The PET data were analyzed using PMOD software (version 3.8; PMOD Technologies Ltd.). PET images were coregistered onto corresponding MR images for each baboon. A baboon T1-weighted MR template (*25*) was normalized onto individual MR images. Transformation matrices were then applied to the segmentation obtained from the template, which included 12 brain structures as volumes of interest: cingulate cortex, orbital cortex, occipital cortex, temporal cortex, frontal cortex, caudate nucleus, putamen, precentral gyrus, postcentral gyrus, thalamus, superior parietal lobe, and cerebellum.

Individual volumes of interest were applied to coregistered dynamic PET images to generate corresponding time–activity curves. Kinetic modeling was performed using a 1-tissue-compartment model (1-TCM) with the corresponding arterial plasma input function of parent ^{11}C-metoclopramide to estimate the influx (K_1; mL/min/cm^3) and efflux (k_2; min^{-1}) rate constants and the total volume of distribution ($V_T = K_1/k_2$ in the 1-TCM; mL/cm^3) for each region under each tested condition. Additional PET kinetic parameters were calculated, including the AUC of regional time–activity curves from 0 to 30 min ($AUC_{0–30\ min}$) and from 30 to 60 min ($AUC_{30–60\ min}$). The elimination slope (k_E; min^{-1}) of ^{11}C-metoclopramide washout from the brain was estimated from the log-transformed time–activity curves from 30 to 60 min after radiotracer injection.

HPLC Determination of Tariquidar in Plasma

Arterial blood samples (3 mL) withdrawn immediately before and during the PET acquisition were used to determine tariquidar concentrations using a newly developed HPLC-ultraviolet method.

Solvents and Chemicals. Elacridar hydrochloride ($C_{34}H_{33}N_3O_5$·HCl; molecular weight, 600.1 g·mol^{-1}), used as an internal standard, was purchased from Syncom. Ultrapure water was obtained using an ultraviolet purification system (Purelab; ELGA LabWater).

HPLC Method. An HPLC-ultraviolet method was developed to determine tariquidar in plasma. HPLC was performed on an Alliance 2996 system (Waters), equipped with an autosampler, a binary pump, and a photodiode array detector. Separation was achieved using an AtlantisT3 C18 column (4.6 × 150 mm, 5 μm; Waters). The mobile phase consisted of water containing 0.1% (v/v) trifluoroacetic acid (solvent A) and acetonitrile containing 0.1% (v/v) trifluoroacetic acid (solvent B) delivered in a gradient elution mode at a flow rate of 1.2 mL·min^{-1}: solvent B increased linearly from 20% to 65% from 0 to 15 min. Tariquidar and the internal standard were detected at a ultraviolet wavelength of 250 nm.

Sample Preparation. Stock solutions of tariquidar and the internal standard were prepared in water/acetonitrile (80/20 and 27/73, v/v, respectively) at a concentration of 1 mg·mL^{-1}. The stock solutions were stored at −20°C.

Arterial and venous blood samples from the animal experiments were collected in tubes containing lithium iodoacetate as an anticoagulant (BD Vacutainer) and were immediately centrifuged for 10 min (2,054*g*, 4°C). The plasma was stored at −80°C until analysis (<1 mo). For analysis, samples were thawed at room temperature. The internal standard solution (diluted with water to a concentration of 60 μg·mL^{-1} [100 μL]) and water containing 4% hydrochloric acid (v/v, 500 μL) were added to the plasma sample (600 μL). After being stirred in a vortex mixer, 1 mL of this mixture was deposited on a cation-exchange solid-phase extraction cartridge (MCX, 30 mg, Oasis; Waters) that had been preconditioned with 1 mL of methanol and 1 mL of water. The cartridge was washed with water containing 0.4% (v/v) hydrochloric acid (1 mL) followed by acetonitrile containing 0.4% (v/v) hydrochloric acid (1 mL). Tariquidar and the internal standard were finally eluted with acetonitrile containing 4% (v/v) ammonia (3 × 1 mL). The combined alkaline acetonitrile fractions were evaporated during 120 min (SPD1010 SpeedVac system; Thermo Scientific). The residue was dissolved in water/acetonitrile/trifluoroacetic acid (80/20/0.5, v/v/v, 100 μL), stirred in a vortex mixer for 30 s, and sonicated for 5 min. This solution (20 μL) was then injected into the HPLC system.

HPLC Determination of Parent ^{11}C-Metoclopramide in Plasma

During the PET experiments, additional plasma samples withdrawn at 0, 5, 10, 15, 30, and 60 min were used to measure the percentage of parent (unmetabolized) ^{11}C-metoclopramide, assessed using radio-HPLC analysis. After centrifugation, the total radioactivity in the plasma samples (500 μL) was counted. Samples were then deproteinated with acetonitrile (700 μL) and centrifuged (5 min, 2,054*g*, 4°C). The pellet of proteins was counted. Recovery of radioactivity in the supernatant was more than 90%. Then, 1,000 μL of the supernatant were injected into the radio-HPLC system.

The radio-HPLC system consisted of a gradient pump, an ASI100T autosampler, and a UVD170U ultraviolet–visible-light detector (Thermo Scientific) in line with a Flo-One scintillation analyzer (Packard). Separation was achieved using an Atlantis T3 5-μm, 10 × 250 mm column (Waters). The mobile phase consisted of 0.1% trifluoroacetic acid in water (solvent A) and acetonitrile (solvent B). A linear gradient from 20% to 40% of solvent B over 9 min was applied to the column at a flow rate of 5 mL/min.

For each experiment, a monoexponential decay function was fitted to the percentage of unmetabolized ^{11}C-metoclopramide versus time and then applied to the corresponding total radioactivity in plasma.

Statistical Analysis

Statistical analysis was performed using GraphPad Prism software (version 7.0). Outcome parameters obtained from pharmacokinetic modeling were compared using 2-way ANOVA. A result was deemed significant when a 2-tailed P value was less than 0.05.

RESULTS

Plasma Pharmacokinetics

Radio-HPLC analysis showed the presence of ^{11}C-metoclopramide and radiometabolites in plasma. In the first 30 min, the parent fraction of ^{11}C-metoclopramide could be determined. After 30 min, the peak corresponding to parent ^{11}C-metoclopramide was below the limit of quantitation and plasma radioactivity consisted of only radiometabolites (Fig. 1). Metabolite-corrected arterial input functions and corresponding AUCs in plasma are thus reported from 0 to 30 min, which corresponds to the time frame allowing for accurate quantitation of parent ^{11}C-metoclopramide in plasma. ^{11}C-metoclopramide plasma kinetics were not affected by tariquidar infusion, with AUCs in plasma of 8.9 ± 4.8 and 9.6 ± 2.9 SUV·min in the baseline and inhibition scans, respectively (P = 0.797). Plasma concentrations peaked rapidly, followed by a fast washout of radioactivity to reach equilibrium (~0.1 SUV) at 10 min after ^{11}C-metoclopramide injection (Fig. 1).

The f_P of ^{11}C-metoclopramide was high in baseline scans (72.2% ± 2.5%), as was consistent with low metoclopramide binding to plasma proteins in humans (*26*). In tariquidar-treated

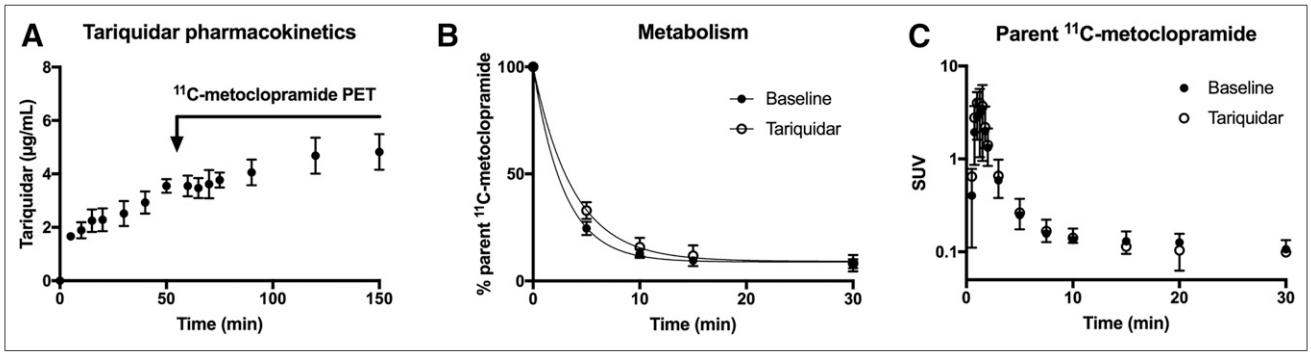

FIGURE 1. Plasma pharmacokinetics of tariquidar and ^{11}C-metoclopramide during PET experiments. (A) Plasma pharmacokinetics of tariquidar (n = 3). (B) f_P of parent ^{11}C-metoclopramide. (C) Arterial input function of parent (unmetabolized) ^{11}C-metoclopramide in animals without (baseline) or with coinfusion of tariquidar (n = 4 for both conditions). Data are mean ± SD.

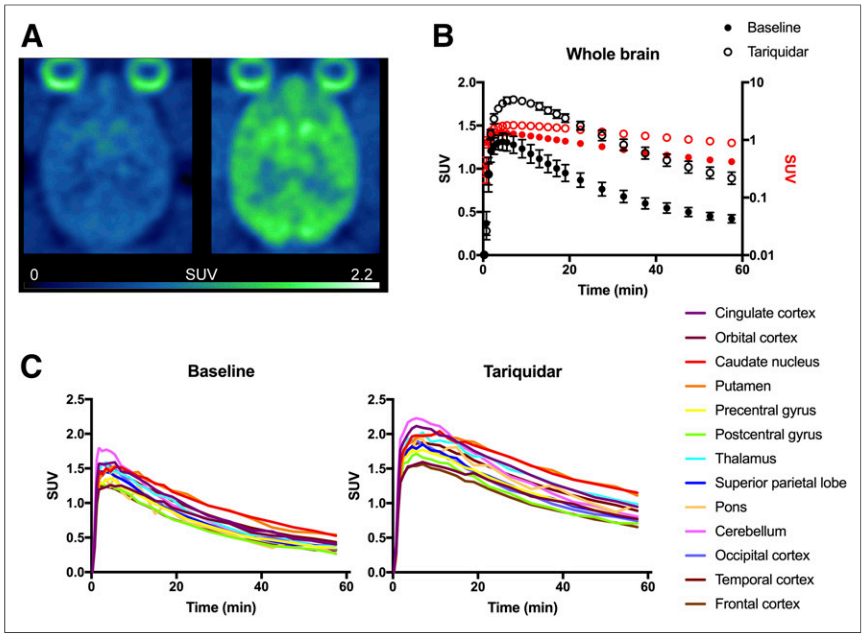

FIGURE 2. ^{11}C-metoclopramide PET data in baboon brain. (A) Representative PET summation images (0–60 min) of brain of baboon without (baseline, left) or with (right) coinfusion of tariquidar. Radioactivity concentration is normalized to injected dose per body weight and expressed as SUV. (B) Mean time–activity curves obtained under both conditions using either linear (black) or logarithmic (red) scale. (C) Regional time–activity curves for both conditions.

animals, f_P was significantly lower (61.6% ± 1.9%; $P < 0.001$, Student t test).

The pharmacokinetics of tariquidar could be measured in only 3 animals because of technical issues. The tariquidar concentration in arterial plasma increased rapidly to reach a range of 3.1–3.9 μg/mL at the start of the PET experiments. The concentration ranged from 4.1 to 5.0 μg/mL at the end of the PET experiments (Fig. 1).

PET Experiments

Baseline PET images showed substantial brain uptake of ^{11}C-metoclopramide–associated radioactivity, which did not accumulate in specific brain regions (Fig. 2). Whole-brain radioactivity peaked rapidly (SUV_{max}, 1.3 ± 0.1; time of maximum uptake, ~4.5 min) followed by a slow decrease, with an SUV of 0.4 ± 0.1 at 60 min after injection (Fig. 2). ABCB1 inhibition resulted in a pronounced and significant increase in SUV_{max} (1.8 ± 0.1, $P < 0.001$) and a delay in the time to maximum uptake, which occurred at about 7 min. The SUV was higher at 60 min (0.9 ± 0.1) than at baseline ($P < 0.001$) (Figs. 1B and 2B). The kinetics of ^{11}C-metoclopramide were similar across different brain regions, in either the presence or the absence of tariquidar (Fig. 2).

The PET data were modeled using a 1-TCM under the 2 tested conditions. The baseline distribution of ^{11}C-metoclopramide to the whole brain (V_T = 4.3 ± 0.5 mL/cm^3; V_T/f_P = 5.9 ± 0.6 mL/cm^3) was significantly increased by ABCB1 inhibition (V_T = 8.7 ± 0.5 mL/cm^3; V_T/f_P = 14.2 ± 0.4 mL/cm^3). Tariquidar induced a significant increase in brain $AUC_{0–30\ min}$ and $AUC_{30–60\ min}$. Estimation of the transfer rate constants for ^{11}C-metoclopramide across the BBB showed a significant increase in K_1, associated with a significant decrease in k_2. The effect of tariquidar on k_2 was consistent with a significant decrease in the elimination slope of radioactivity from the brain (k_E) from 30 to 60 min (Fig. 3; Supplemental Table 1).

For all outcome parameters (V_T, K_1, k_2, k_E, $AUC_{0–30\ min}$, and $AUC_{30–60\ min}$), the response to ABCB1 inhibition did not significantly differ among brain regions (P = 0.14), suggesting that the impact of tariquidar on ABCB1 function was homogeneous in the different brain regions. The impact of tariquidar was highest on V_T and $AUC_{30–60\ min}$ and lowest on K_1 and k_E (Fig. 3; Supplemental Table 1). The variability in response to tariquidar was highest for K_1 (coefficient of variation, 51%) and lowest for $AUC_{30–60\ min}$ (9%) and k_E (11%) (Fig. 3).

The brain distribution of ^{11}C-metoclopramide (V_T), estimated in each region from 0 to 30 min, was used as a reference parameter to evaluate simplified methods to quantify ABCB1 function at the BBB. A significant correlation was found between V_T and $AUC_{0–30\ min}$ ($P < 0.0001$; r^2 = 0.87) and between V_T and $AUC_{30–60\ min}$ (r^2 = 0.95). The k_E of the regional time–activity curves from 30 to 60 min correlated with V_T and k_2 ($P < 0.0001$; r^2 = 0.62) (Fig. 4).

DISCUSSION

PET imaging using radiolabeled ABCB1 substrates convincingly highlighted the importance of ABCB1 for drug distribution to the brain in animals and humans (*2*). The currently available PET probes revealed and quantified the influx hindrance (K_1) component of ABCB1. In this study, ^{11}C-metoclopramide PET imaging and kinetic modeling were performed on nonhuman primates to gain information about the kinetic role of ABCB1 on the brain distribution of a weak ABCB1 substrate.

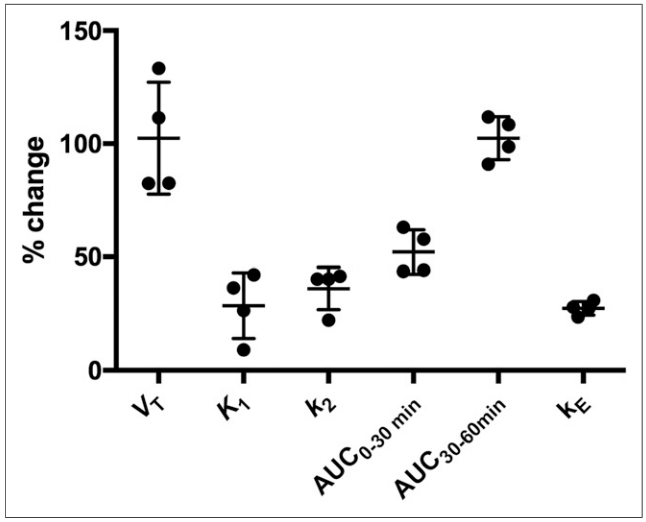

FIGURE 3. Impact of ABCB1 inhibition on ^{11}C-metoclopramide pharmacokinetic parameters. Percentage change in each parameter in whole brain in inhibition scan relative to baseline scan is reported. Data are individual values, as well as mean ± SD over 4 baboons.

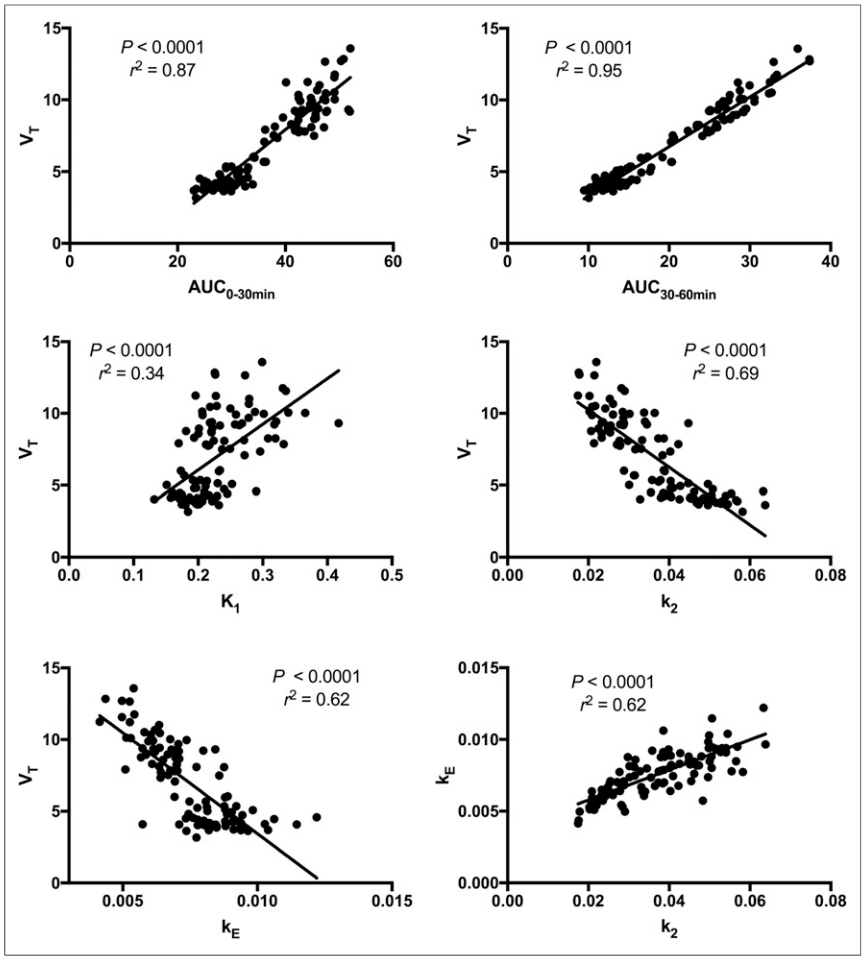

FIGURE 4. Correlations between different parameters describing kinetics of ^{11}C-metoclopramide in brain. Regional outcome parameter values obtained in 4 animals in presence and absence of ABCB1 inhibition are plotted. Linear regression analysis was performed. Statistical significance and goodness of fit (r^2) are reported for each correlation.

^{11}C-metoclopramide benefits from favorable pharmacokinetic properties that allow for quantitative determination of modeling outcome parameters describing its brain distribution. ^{11}C-metoclopramide behaves like a weak substrate for ABCB1, with substantial brain uptake (baseline V_T = 4.3 mL/cm^3) despite fully functional ABCB1 activity. In vitro experiments have shown that ^{11}C-metoclopramide is specifically transported by human ABCB1 but not ABCG2, the other major ABC transporter expressed at the human BBB (*19*). In rats, the BBB was poorly crossed by ^{11}C-metoclopramide radiometabolites, compared with the parent compound, thus ensuring the radiochemical purity of the PET signal in the brain even when ABCB1 was inhibited (*19*).

In nonhuman primates, the brain kinetics of a tracer dose of ^{11}C-metoclopramide could be described by a simple 1-TCM. This model allows for the estimation of rate constants to describe the exchange of ^{11}C-metoclopramide–associated radioactivity between the plasma and the brain compartments (*27*). Metoclopramide is a dopamine D_2 receptor antagonist and was expected to bind to dopamine D_2 receptors in the brain (*28*). In our study, radioactivity was homogeneously distributed among brain regions and did not predominantly accumulate in dopamine D_2 receptor–rich regions such as the striatum (Fig. 2). Our previous rat experiments have shown that ABCB1 inhibition resulted in a significant increase in ^{11}C-metoclopramide nondisplaceable binding potential in the whole brain, estimated using a 2-tissue-compartment model (2-TCM). However, injection of a high dose of unlabeled metoclopramide during the PET scan did not displace the brain radioactivity, suggesting that receptor binding is not the main mechanism for ^{11}C-metoclopramide retention in the brain (*19*). In our nonhuman primate study, the 2-TCM model did not allow for accurate estimation of ^{11}C-metoclopramide nondisplaceable binding potential and was therefore not used. Coinjection of unlabeled metoclopramide had no impact on ^{11}C-metoclopramide brain kinetics (Supplemental Fig. 1). The mechanism of ^{11}C-metoclopramide retention in the brain remains to be elucidated to determine a possible interference with quantification of ABCB1 function at the BBB in different pathophysiologic conditions.

We chose a clinically feasible infusion protocol for tariquidar to highlight the impact of impaired ABCB1 function on the brain kinetics of ^{11}C-metoclopramide (*14*). This protocol allowed for maintained and controlled plasma concentrations during the PET experiments to limit any variation in ABCB1 function. ABCB1 inhibition induced a significant, approximately 2-fold, increase in the V_T of ^{11}C-metoclopramide. Tariquidar did not cause any change in the arterial input function and did not increase the ^{11}C-metoclopramide f_P (*23*). As a consequence, V_T significantly correlated with the concomitant brain exposure ($AUC_{0–30\ min}$; Fig. 4).

Pharmacokinetic modeling revealed that ABCB1 induced a significant 28.5% increase in K_1. This effect corresponds to the influx hindrance component of ABCB1 function at the BBB. Compared with established avid ABCB1 PET probes, this effect was modest, as might be explained by the lower transport ability of metoclopramide by ABCB1 or a higher passive diffusion component of the baseline ^{11}C-metoclopramide transport across the BBB (*12*). ABCB1 inhibition also induced a concomitant 36% decrease in k_2. This result shows that once in the brain, ABCB1 can mediate clearance of its substrates back into the blood compartment. From a pharmacokinetic perspective, the efflux enhancement function of ABCB1 (described by k_2), in addition to its effect on initial uptake (described by K_1), accounts for the overall brain exposure (described by V_T and AUC), which was increased by approximately 2-fold after ABCB1 inhibition (*29*).

The in vitro transport of solutes across cell monolayers with polarized (apical) ABCB1 expression shows that the predominant impact of ABCB1 is usually along the concentration gradient (basolateral-to-apical) rather than against the concentration gradient (apical-to-basolateral) (*10,12*). This finding suggests that ABCB1 is more efficient in promoting efflux clearance than in competing with passive diffusion to limit the net influx across

biologic barriers (*10,12*). In vivo, the efflux enhancement component of ABCB1 at the BBB has been suggested from invasive experiments. The brain efflux index can be assessed by injecting solutes into the brain and measuring the remaining brain concentrations during washout (*30*). Brain microdialysis allows for concomitant consideration of the brain and plasma kinetics of solutes and estimation of the corresponding transfer constant (*13*). Our PET data suggest an efflux-component role for ^{11}C-metoclopramide distribution across the BBB, but the presence of brain radiometabolites prevented us from addressing this role using ^{11}C-verapamil PET imaging. ^{11}C-*N-desmethyl*-loperamide was shown to be trapped in brain cells, and the radiotracer may therefore not be available for ABCB1-mediated brain clearance in vivo (*31*).

The ABCB1-mediated efflux clearance could also be intuitively estimated from the Log-transformed brain time–activity curves for ^{11}C-metoclopramide. Thirty minutes after injection, ^{11}C-metoclopramide–associated radioactivity was about 7-fold higher in the brain than in plasma when ABCB1 was fully functional. Thereafter, parent ^{11}C-metoclopramide could not be detected in plasma anymore. This situation is similar to the kinetic properties of ^{99m}Tc-sestamibi, for which the efflux rate was shown to be more accurate than the initial uptake in predicting ABCB1-mediated multidrug resistance in patients (*32*).

We sought to propose simplified parameters for quantitative estimation of the role of ABCB1 in the brain kinetics of ^{11}C-metoclopramide. Using V_T as a reference parameter, brain AUC was investigated as a surrogate parameter, as previously reported for ^{11}C-*N-desmethyl*-loperamide (*33*). We found a better correlation between V_T and $AUC_{30–60\ min}$ than between V_T and $AUC_{0–30\ min}$, the latter being more likely dependent on the variability in plasma and brain kinetics at early time points. $AUC_{30–60\ min}$ should preferentially be used as a surrogate parameter to describe V_T, as $AUC_{30–60\ min}$ reflects the impact of ABCB1 on the overall brain exposure to ^{11}C-metoclopramide without the need for an arterial input function. Interestingly, k_E correlated with V_T and k_2 (Fig. 4). k_E depends neither on the arterial input nor on the initial uptake of the radiotracer and corresponding SUV_{max}. Moreover, a low variability in the response of k_E to ABCB1 inhibition was observed (Fig. 4). In some situations, k_E may therefore be preferred as a pharmacokinetically relevant outcome parameter to noninvasively describe and quantify the efflux enhancement role of ABCB1 at the BBB.

Tracer-dose ^{11}C-metoclopramide PET imaging can be safely and noninvasively performed on humans with or without ABCB1 inhibition. Compared with existing radiotracers, the lower transport rate of ^{11}C-metoclopramide by ABCB1 may offer new opportunities for the study of ABCB1 function at the BBB. Further investigations are thus needed to assess the sensitivity of ^{11}C-metoclopramide PET in detecting the functional impact of disease-induced reduction or induction of ABCB1 at the BBB (*34*).

CONCLUSION

We performed ^{11}C-metoclopramide PET imaging and pharmacokinetic modeling on baboons to validate simplified methods for quantification of ABCB1 function at the BBB for practical clinical use. ^{11}C-metoclopramide PET imaging provides novel insight into the kinetic impact of ABCB1 at the BBB on brain distribution of weak substrates.

DISCLOSURE

No potential conflict of interest relevant to this article was reported.

ACKNOWLEDGMENTS

We thank Thierry Lekieffre, Maud Goislard, and Vincent Brulon for helpful technical assistance.

REFERENCES

1. Schinkel AH, Smit JJ, van Tellingen O, et al. Disruption of the mouse mdr1a P-glycoprotein gene leads to a deficiency in the blood-brain barrier and to increased sensitivity to drugs. *Cell.* 1994;77:491–502.
2. Kannan P, John C, Zoghbi SS, et al. Imaging the function of P-glycoprotein with radiotracers: pharmacokinetics and in vivo applications. *Clin Pharmacol Ther.* 2009;86:368–377.
3. Abbott NJ, Patabendige AAK, Dolman DEM, Yusof SR, Begley DJ. Structure and function of the blood-brain barrier. *Neurobiol Dis.* 2010;37:13–25.
4. Giacomini KM, Huang S-M, Tweedie DJ, et al. Membrane transporters in drug development. *Nat Rev Drug Discov.* 2010;9:215–236.
5. Schinkel AH, Wagenaar E, Mol CA, van Deemter L. P-glycoprotein in the blood-brain barrier of mice influences the brain penetration and pharmacological activity of many drugs. *J Clin Invest.* 1996;97:2517–2524.
6. Luna-Tortós C, Fedrowitz M, Löscher W. Several major antiepileptic drugs are substrates for human P-glycoprotein. *Neuropharmacology.* 2008;55:1364–1375.
7. Tournier N, Declèves X, Saubaméa B, Scherrmann J-M, Cisternino S. Opioid transport by ATP-binding cassette transporters at the blood-brain barrier: implications for neuropsychopharmacology. *Curr Pharm Des.* 2011;17:2829–2842.
8. O'Brien FE, Dinan TG, Griffin BT, Cryan JF. Interactions between antidepressants and P-glycoprotein at the blood-brain barrier: clinical significance of in vitro and in vivo findings. *Br J Pharmacol.* 2012;165:289–312.
9. Loryan I, Melander E, Svensson M, et al. In-depth neuropharmacokinetic analysis of antipsychotics based on a novel approach to estimate unbound target-site concentration in CNS regions: link to spatial receptor occupancy. *Mol Psychiatry.* 2016;21:1527–1536.
10. Feng B, Mills JB, Davidson RE, et al. In vitro P-glycoprotein assays to predict the in vivo interactions of P-glycoprotein with drugs in the central nervous system. *Drug Metab Dispos.* 2008;36:268–275.
11. Doran A, Obach RS, Smith BJ, et al. The impact of P-glycoprotein on the disposition of drugs targeted for indications of the central nervous system: evaluation using the MDR1A/1B knockout mouse model. *Drug Metab Dispos.* 2005;33:165–174.
12. Mahar Doan KM, Humphreys JE, Webster LO, et al. Passive permeability and P-glycoprotein-mediated efflux differentiate central nervous system (CNS) and non-CNS marketed drugs. *J Pharmacol Exp Ther.* 2002;303:1029–1037.
13. Syvänen S, Xie R, Sahin S, Hammarlund-Udenaes M. Pharmacokinetic consequences of active drug efflux at the blood-brain barrier. *Pharm Res.* 2006;23:705–717.
14. Bauer M, Karch R, Zeitlinger M, et al. Approaching complete inhibition of P-glycoprotein at the human blood-brain barrier: an (R)-[^{11}C]verapamil PET study. *J Cereb Blood Flow Metab.* 2015;35:743–746.
15. Kreisl WC, Bhatia R, Morse CL, et al. Increased permeability-glycoprotein inhibition at the human blood-brain barrier can be safely achieved by performing PET during peak plasma concentrations of tariquidar. *J Nucl Med.* 2015;56:82–87.
16. Chaves C, Shawahna R, Jacob A, Scherrmann J-M, Declèves X. Human ABC transporters at blood-CNS interfaces as determinants of CNS drug penetration. *Curr Pharm Des.* 2014;20:1450–1462.
17. Rao AS, Camilleri M. Review article: metoclopramide and tardive dyskinesia. *Aliment Pharmacol Ther.* 2010;31:11–19.
18. Liu X, Van Natta K, Yeo H, et al. Unbound drug concentration in brain homogenate and cerebral spinal fluid at steady state as a surrogate for unbound concentration in brain interstitial fluid. *Drug Metab Dispos.* 2009;37:787–793.
19. Pottier G, Marie S, Goutal S, et al. Imaging the impact of the P-glycoprotein (ABCB1) function on the brain kinetics of metoclopramide. *J Nucl Med.* 2016;57:309–314.
20. Uchida Y, Wakayama K, Ohtsuki S, et al. Blood-brain barrier pharmacoproteomics-based reconstruction of the in vivo brain distribution of P-glycoprotein substrates in cynomolgus monkeys. *J Pharmacol Exp Ther.* 2014;350:578–588.

21. Caillé F, Goutal S, Marie S, et al. Positron emission tomography imaging reveals an importance of saturable liver uptake transport for the pharmacokinetics of metoclopramide. *Contrast Media Mol Imaging*. 2018;2018:7310146.
22. Auvity S, Saba W, Goutal S, et al. Acute morphine exposure increases the brain distribution of [^{18}F]DPA-714, a PET biomarker of glial activation in nonhuman primates. *Int J Neuropsychopharmacol.* 2017;20:67–71.
23. Tournier N, Cisternino S, Peyronneau M-A, et al. Discrepancies in the P-glycoprotein-mediated transport of ^{18}F-MPPF: a pharmacokinetic study in mice and non-human primates. *Pharm Res.* 2012;29:2468–2476.
24. Tournier N, Goutal S, Auvity S, et al. Strategies to inhibit ABCB1- and ABCG2-mediated efflux transport of erlotinib at the blood-brain barrier: a PET study on nonhuman primates. *J Nucl Med.* 2017;58:117–122.
25. Black KJ, Snyder AZ, Koller JM, Gado MH, Perlmutter JS. Template images for nonhuman primate neuroimaging: 1. Baboon. *Neuroimage.* 2001;14:736–743.
26. Webb D, Buss DC, Fifield R, Bateman DN, Routledge PA. The plasma protein binding of metoclopramide in health and renal disease. *Br J Clin Pharmacol.* 1986;21:334–336.
27. Innis RB, Cunningham VJ, Delforge J, et al. Consensus nomenclature for in vivo imaging of reversibly binding radioligands. *J Cereb Blood Flow Metab.* 2007;27:1533–1539.
28. Woodward R, Daniell SJ, Strange PG, Naylor LH. Structural studies on D2 dopamine receptors: mutation of a histidine residue specifically affects the binding of a subgroup of substituted benzamide drugs. *J Neurochem.* 1994;62:1664–1669.
29. Terasaki T, Hosoya K. The blood-brain barrier efflux transporters as a detoxifying system for the brain. *Adv Drug Deliv Rev.* 1999;36:195–209.
30. Kusuhara H, Suzuki H, Terasaki T, Kakee A, Lemaire M, Sugiyama Y. P-glycoprotein mediates the efflux of quinidine across the blood-brain barrier. *J Pharmacol Exp Ther.* 1997;283:574–580.
31. Kannan P, Brimacombe KR, Kreisl WC, et al. Lysosomal trapping of a radiolabeled substrate of P-glycoprotein as a mechanism for signal amplification in PET. *Proc Natl Acad Sci USA.* 2011;108:2593–2598.
32. Taki J, Sumiya H, Asada N, Ueda Y, Tsuchiya H, Tonami N. Assessment of P-glycoprotein in patients with malignant bone and soft-tissue tumors using technetium-99m-MIBI scintigraphy. *J Nucl Med.* 1998;39:1179–1184.
33. Kreisl WC, Liow J-S, Kimura N, et al. P-glycoprotein function at the blood-brain barrier in humans can be quantified with the substrate radiotracer ^{11}C-N-desmethyl-loperamide. *J Nucl Med.* 2010;51:559–566.
34. Miller DS. Regulation of ABC transporters blood-brain barrier: the good, the bad, and the ugly. *Adv Cancer Res.* 2015;125:43–70.